

Survivability Simulation of Airborne Platform With Expendable Active Decoy Countering RF Missile

JAE-WON RIM 

Inha University, Incheon, South Korea

IL-SUEK KOH 

Inha University, Incheon, South Korea

By employing an expendable repeater-type decoy that is known as efficient electronic countermeasure device, the survivability of an airborne platform can be improved. To optimize the survivability of the aircraft by managing the active decoy, analyzing which factors critically affect to the survivability is very important. For its dynamic situation, where the motions and interaction of the decoy, platform, and missile varied with respect to time, a modeling and simulation (M&S) approach is preferred, which can consider other factors: radio frequency specification of decoy, guidance model of the missile, and so on. Based on the proposed M&S approach, several crucial factors affecting to the survivability of the platform such as platform reaction range, platform maneuvering, decoy dynamics, missile's maximum load factor, etc., are addressed and numerically analyzed. Additionally, the survival probability of the platform is also simulated on several engagement scenarios through the Monte Carlo simulation.

Manuscript received May 18, 2018; revised September 9, 2018 and December 17, 2018; released for publication April 5, 2019. Date of publication April 29, 2019; date of current version February 7, 2020.

DOI. No. 10.1109/TAES.2019.2913722

Refereeing of this contribution was handled by P. E. Pace.

This work was supported in part by the Electronic Warfare Research Center, Gwangju Institute of Science and Technology, originally funded by Defense Acquisition Program Administration, and in part by the Agency for Defense Development.

Author's address: J.-W. Rim is with the Department of Electronic Engineering, Inha University, Incheon 22212, South Korea, E-mail: (jwr@inha.edu); I.-S. Koh is with the Department of Electronic Engineering, Inha University, Incheon 22212, South Korea, E-mail: (ikoh@inha.ac.kr). Corresponding author: Il-Suek Koh.

0018-9251 © 2019 IEEE

I. INTRODUCTION

A preponderant aspect in the survivability of an aircraft is its defense against hostile radio frequency (RF) missile systems [1]. The RF missile, with its superior properties, including its wide bandwidth, high velocity, and high sensitivity can be a lethal threat to an aircraft. However, RF missile designs that determine the range and angle of attack by processing RF echo signals from a target aircraft were found vulnerable to airborne defensive electronic counter-measure (ECM) techniques.

Among numerous ECM techniques, expendable repeater-type decoys, which are usually ejected from an aircraft to reradiate decoying signals after amplifying received signals, have been considered as one of the most effective countermeasures. The advantage of repeater-type ECMs is represented by its relatively low cost and the fact that several expendables stored in the aircraft can counter multiple attacks [2].

To optimize the survivability of the aircraft with expendable active decoys, analyzing which factors critically affect to the survivability is very important. For this, an efficient modeling and simulation (M&S) approach is definitely required because analyzing the performance of decoy systems on various engagement scenarios is considerably challenging, and it is not efficient to analyze multiple situations through experiments. To mimic realistic combat scenarios, the M&S approach should incorporate the following details: First, the dynamics of the decoy and airborne platform are important because their positions and directions continuously vary. The movement of the decoy depends on the aircraft motion because it is interfered by the airflow around the aircraft. Second, the RF missile and RF specifications of the decoy, such as antenna patterns, polarizations, and propagation characteristics are essential because the echo jamming capability depends on these specifications. Third, the aircraft's two-dimensional (2-D) polarimetric monostatic scattering matrices, which are evaluated considering the geometry of the aircraft, affect the scattered power from the aircraft. Finally, the radar signal processing of the RF missile and guidance modules should be accurately considered when echo signals for every pulse repetition time vary according to the situation, and the missile is guided based on the processing results of the echo signal.

Several publications have reported on various numerical approaches for analyzing the jamming performance of decoy systems [3]–[7]. However, the topics in [3] and [4] are focused, not on expendable decoys, but on towed decoys. Moreover, their theoretical models in [3] and [4] do not include the details mentioned above. Theoretical models presented in [5] and [6] address similar M&S approaches. However, difference considerations are incorporated because scenarios and problems of interest are different with ours. For example, Zhou [5] considered an antiradiation missile (ARM) attacking an active RF source, which is capable of analyzing the survival probability of an aircraft, considering several details, such as beam patterns, polarizations, and propagation characteristics. Lakshmi [6]

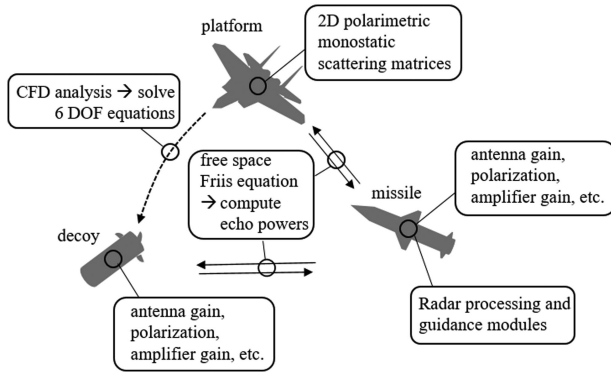


Fig. 1. Summary of modeling and simulation approach on deployment scenario.

analyzed the survivability and miss distance in situations involving a decoy launched from a ship to counter an incoming missile where optimal launch angles of the decoy are simulated. However, the studies in [5] and [6] adopted simplified dynamic model as well as they did not encompass the monostatic radar cross section (RCS) of the aircraft into the model because considered scenarios were different with ours. In our previous work in [7], we have proposed a numerical approach that considers all of the aforementioned details in order to analyze the jamming performance of expendable decoys. However, the analysis was restricted to countering a ground-based tracking radar, and the deception (or soft kill) performance against an RF missile system was not taken into consideration. Analyzing significant parameters increasing the survivability of the airborne platform against oncoming RF missile system such as platform maneuverings, decoy dynamics, RF specifications of decoy, etc., is very important since the analysis enables optimal design of the decoy and optimal management of the platform.

In Section II, this paper describes the M&S approach, where the deployment scenario is summarized and modeling of the RF missile is explained in detail. Several important problems resolved under some deployment scenarios and the analysis of the decoy's ECM performance are presented in Section III. Finally, conclusions are summarized in Section IV.

II. MODELING AND SIMULATION APPROACH

A. Summary of M&S Approach

Fig. 1 summarizes the M&S approach on a deployment scenario, where an airborne platform, expendable decoy, and RF missile were under dynamic states. The RF missile was initially launched toward the intercept point, whereas its antenna beam was steered toward the platform. To counteract the incoming missile, a decoy was ejected by the platform to delude the missile, and an evasion flight was executed to improve its survivability. The trajectory of the decoy was dependent on the movement of the platform and its initial ejection condition because aerodynamic forces and moments of the decoy were strongly influenced by

airflows around the platform. Hence, computational fluid dynamics analysis was exploited to accurately compute the interfering flow field around the platform. It was on this analysis that the solution of a six-degree-of-freedom equation was based [8]. The RF missile transmitted a chirp signal every pulse repetition time (PRT) and, thereafter, received echo signals from two bodies: the platform and decoy. The accurate evaluation of time-domain echo signals during the PRT was considerably important because it significantly affected the estimation and guidance results of the missile. Because the repeater-type decoy that amplified and reraided the received signal was considered, the decoy's RF system was simply modeled as a combination of an antenna and a power amplifier. For the accurate computation of the echo power from the platform, 2-D fully polarimetric monostatic scattering matrices were derived as a function of two incidence angles. The scattering made by the decoy body was ignored because its effective reflection area was negligibly small compared to that of the platform. Because most of the energy of the echo signal was received by the main beam for the considered scenario, the RF channel between the platform and missile can be assumed as a free space. Thus, the free-space Friis transmission formula was employed to compute the echo signal [9]. The movement of each object between PRT intervals was negligible because, in general, PRT was considerably brief. Hence, the formulations in [7] were used to compute the radar echo signal of every missile PRT. The modeling of the radar signal processing and guidance modules of the missile are described in the following section.

B. Active RF Missile Model

Modern missile systems transmit linear frequency modulated waveforms to resolve targets with high resolutions. The chirp waveform is expressed as

$$r(t) = \exp \left[j2\pi \left(f_0 t + \frac{\mu}{2} t^2 \right) \right] \text{rect} \left(\frac{t}{\tau} \right) \quad (1)$$

where f_0 , τ , and μ are the center frequency, pulsewidth, and chirp rate, respectively; t is the fast time between PRT intervals; $\text{rect}(\cdot)$ is the rectangular function. Based on the jamming power from the decoy, J , and the scattered power from the platform S , at the n th PRT, the time-domain echo signal can be expressed as

$$\begin{aligned} s(t) &\approx \text{ARF}(\theta_0^{(n)}, \phi_0^{(n)}, \theta_p^{(n)}, \phi_p^{(n)}) \sqrt{S^{(n)}} \\ &\times r \left(t - nT - \frac{2R_p^{(n)}}{c} \right) \\ &+ \text{ARF}(\theta_0^{(n)}, \phi_0^{(n)}, \theta_d^{(n)}, \phi_d^{(n)}) \sqrt{J^{(n)}} \\ &\times r \left(t - nT - \frac{2R_d^{(n)}}{c} \right). \end{aligned} \quad (2)$$

Here, the echo powers are assumed to be constant over the chirp bandwidth, and J and S can be evaluated based on the Friis transmission formula, as explained in [7]. Note that the polarimetric scattering matrices of the platform is required to compute S in which we adopted the shooting and

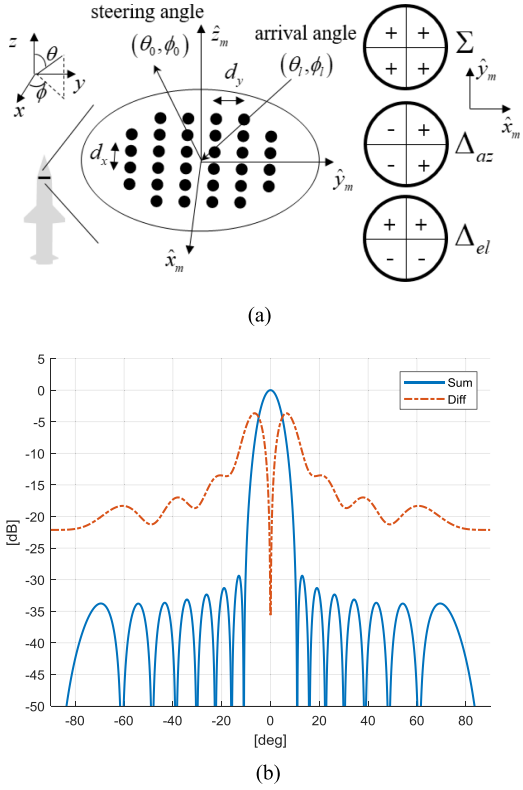


Fig. 2. (a) Antenna geometry. (b) Normalized sum and difference patterns.

bouncing ray technique to evaluate the scattering matrices at the frequency of 16 GHz. The superscript n indicates the n th PRT; θ_l and ϕ_l ($l = p$ or d) are elevation and azimuth angles, respectively, related to the platform, for $l = p$, and to the decoy, for $l = d$, in each local coordinate system [see Fig. 2(a)]; θ_0 and ϕ_0 are the antenna beam steering angles; R_p and R_d are distances from the missile to the platform and decoy, respectively. In (2), $\text{ARF}(\cdot, \cdot, \cdot, \cdot)$ is the array factor of the missile's antenna, expressed as

$$\begin{aligned} \text{ARF}(\theta_l, \phi_l, \theta_0, \phi_0) = & \sum_{a \in R} \sum_{b \in R} w_{a,b} \exp \\ & \times [-jk_0 d_x(u_l - u_0) - jk_0 d_y(v_l - v_0)] \end{aligned} \quad (3)$$

where $u_{l,0} = \sin \theta_{l,0} \cos \phi_{l,0}$ and $v_{l,0} = \sin \theta_{l,0} \sin \phi_{l,0}$; k_0 is the free-space propagation constant; d_x and d_y are the spacing between antenna elements, as shown in Fig. 2(a).

Depending on the weights of antenna elements, $w_{a,b}$, the antenna array factor, $\text{ARF}(\cdot, \cdot, \cdot, \cdot)$, was transformed into the sum (Σ) or two difference patterns (Δ_{el} and Δ_{az}). In this study, the amplitude comparison monopulse system was assumed, in which the arrival angles were calculated based on the amplitude ratios between the difference and sum patterns [10]. The amplitude comparison monopulse system had different antenna weights in four quadrants, as depicted in Fig. 2(a). The sum and difference patterns are shown in Fig. 2(b), where 232 antenna elements were modeled as a circular grid array with a half-wavelength spacing, and their magnitudes were tapered based on Taylor's series. By using the sum and two antenna patterns, a sum signal

($s^\Sigma(t)$) and difference signal ($s^{\Delta_{el}}(t)$ and $s^{\Delta_{az}}(t)$) can be calculated by (2). After the down conversion, the compressed baseband sum and difference signals were sampled as $s_c^\Sigma[k]$, $s_c^{\Delta_{el}}[k]$, and $s_c^{\Delta_{az}}[k]$ [11]. The compressed sum signal $s_c^\Sigma[k]$ was used to detect and estimate the target range $\tilde{R}^{(n)}$ and determine the local maximum index k_{\max} . The monopulse ratio for this index approximated the half power beamwidth (HPBW) by [10]

$$\begin{aligned} \frac{s_c^{\Delta_{az}}[k_{\max}]}{s_c^\Sigma[k_{\max}]} &= j \tan \left(\frac{\sin \delta\theta \cos \delta\phi}{2} \right) \approx j k_{az} \delta\phi \\ \frac{s_c^{\Delta_{el}}[k_{\max}]}{s_c^\Sigma[k_{\max}]} &= j \tan \left(\frac{\sin \delta\theta \sin \delta\phi}{2} \right) \approx j k_{el} \delta\theta \end{aligned} \quad (4)$$

where $\delta\theta$ and $\delta\phi$ are offset angles of the target from the beam steering angles θ_0 and ϕ_0 , respectively; k_{el} and k_{az} are the angle sensitivity coefficients, depending on the antenna configuration [10]. The angles $\delta\theta$ and $\delta\phi$ can be computed as follows:

$$\delta\phi = \frac{-j s_c^{\Delta_{az}}[k_{\max}]}{k_{az} s_c^\Sigma[k_{\max}]}, \quad \delta\theta = \frac{-j s_c^{\Delta_{el}}[k_{\max}]}{k_{el} s_c^\Sigma[k_{\max}]} \quad (5)$$

After computing $\delta\theta$ and $\delta\phi$ in (5), the estimated arrival angles $\tilde{\theta}^{(n)}$ and $\tilde{\phi}^{(n)}$ were represented as

$$\tilde{\theta}^{(n)} = \theta_0^{(n)} + \delta\theta^{(n)}; \quad \tilde{\phi}^{(n)} = \phi_0^{(n)} + \delta\phi^{(n)} \quad (6)$$

From $\tilde{R}^{(n)}$, $\tilde{\theta}^{(n)}$, and $\tilde{\phi}^{(n)}$ defined in the missile's local coordinates, the 3-D target position $\tilde{r}_0^{(n)}$ in global coordinates should be converted as

$$\begin{aligned} \tilde{r}_0^{(n)} = \tilde{r}_0(nT) = & (\tilde{R}^{(n)} \sin \tilde{\theta}^{(n)} \cos \tilde{\phi}^{(n)}) \hat{x}_m^{(n)} \\ & + (\tilde{R}^{(n)} \sin \tilde{\theta}^{(n)} \sin \tilde{\phi}^{(n)}) \hat{y}_m^{(n)} + (\tilde{R}^{(n)} \cos \tilde{\theta}^{(n)}) \hat{z}_m^{(n)} \end{aligned}$$

where \hat{x}_m , \hat{y}_m , and \hat{z}_m indicate local coordinates of the missile (see Fig. 2). For the prediction and smoothing of the observed vector $\tilde{r}_0^{(n)}$ an $\alpha\beta\gamma$ tracking filter was used [12]. After the n th observation, the $\alpha\beta\gamma$ filter evaluated the smoothed position $\tilde{r}_s^{(n)}$, velocity $\dot{\tilde{r}}_s^{(n)}$, and acceleration $\ddot{\tilde{r}}_s^{(n)}$, as follows:

$$\tilde{r}_s^{(n)} = \tilde{r}_p^{(n)} + \alpha(\tilde{r}_0^{(n)} - \tilde{r}_p^{(n)}) \quad (7)$$

$$\dot{\tilde{r}}_s^{(n)} = \dot{\tilde{r}}_s^{(n-1)} + T \ddot{\tilde{r}}_s^{(n-1)} + \frac{\beta}{T}(\tilde{r}_0^{(n)} - \tilde{r}_p^{(n)}) \quad (8)$$

$$\ddot{\tilde{r}}_s^{(n)} = \ddot{\tilde{r}}_s^{(n-1)} + \frac{2\gamma}{T^2}(\tilde{r}_0^{(n)} - \tilde{r}_p^{(n)}) \quad (9)$$

$$\tilde{r}_p^{(n+1)} = \tilde{r}_s^{(n)} + T \dot{\tilde{r}}_s^{(n)} + \frac{T^2}{2} \ddot{\tilde{r}}_s^{(n)} \quad (10)$$

where $\tilde{r}_0^{(n)}$ and $\tilde{r}_p^{(n)}$ are the observed and predicted target positions, respectively. Note that the n th observation indicates the n th PRT nT . The initial conditions for (6)–(9) were assumed as $\tilde{r}_s^{(1)} = \tilde{r}_p^{(2)} = \tilde{r}_0^{(1)}$, $\dot{\tilde{r}}_s^{(1)} = \dot{\tilde{r}}_s^{(2)} = \tilde{r}_0^{(2)} = 0$, and $\ddot{\tilde{r}}_s^{(2)} = (\tilde{r}_0^{(2)} - \tilde{r}_0^{(1)})/T$. The gains, α , β , and γ were determined by the smoothing coefficient ξ as $\alpha = 1 - \xi^3$, $\beta = 1.5(1 - \xi)^2(1 + \xi)$, and $\gamma = (1 - \xi)^3$, where $0 \leq \xi \leq 1$. The smoothed position and velocity were used to guide the missile toward the target, and the proportional navigation (PN) guidance law was adopted [13]. Based on the PN

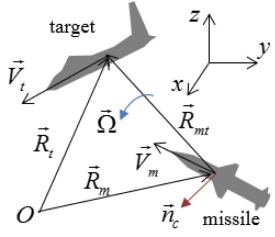


Fig. 3. Three-dimensional missile-target engagement geometry.

method, the missile velocity vector was rotated at a rate proportional to the rotation rate of the line of sight (LOS) [13], as depicted in Fig. 3. The target position, target velocity, missile position, and missile velocity were denoted by \vec{R}_t , \vec{V}_t , \vec{R}_m , and \vec{V}_m , respectively. As \vec{R}_m and \vec{V}_m were determined, \vec{R}_t and \vec{V}_t should be estimated as $\vec{R}_t^{(n)} = \vec{r}_s^{(n)}$ and $\vec{V}_t^{(n)} = \vec{r}_s^{(n)}$, respectively, which can be extracted from the $\alpha\beta\gamma$ filter.

In the PN guidance, an acceleration command vector of the missile, \vec{n}_c , was calculated as

$$\vec{n}_c = N_p \left| \vec{V}_{mt} \right| \vec{\Omega} \times \frac{\vec{R}_{mt}}{\left| \vec{R}_{mt} \right|} \quad (11)$$

where $\vec{V}_{mt} = \vec{V}_t - \vec{V}_m$ and $\vec{R}_{mt} = \vec{R}_t - \vec{R}_m$; N_p is the proportionality constant having an integer value, which is 3–5 in general. In our simulation, N_p is set to four. The rotation vector $\vec{\Omega}$ is represented as $\vec{\Omega} = (\vec{R}_{mt} \times \vec{V}_{mt}) / (\vec{R}_{mt} \cdot \vec{V}_{mt})$. Based on \vec{n}_c , the missile recursively modified its velocity vector every PRT, which guided the missile toward the target. The iterative process was as follows:

$$\vec{R}_m^{(n+1)} = \vec{R}_m^{(n)} + T \vec{V}_m^{(n)} + 0.5T^2 \vec{n}_c^{(n)} \quad (12)$$

$$\vec{V}_m^{(n+1)} = \vec{V}_m^{(n)} + T \vec{n}_c^{(n)}. \quad (13)$$

The maximum value of $|\vec{n}_c|$ in (11), called maximum load factor, was generally limited. Here, the maximum load factor of the missile was set to 12g, where $g = 9.81 \text{ m/s}^2$ [13].

C. Dynamic Simulation Procedure

The flow chart for the time-domain simulation is shown in Fig. 4. From the initial condition, each object (platform, decoy, and missile) updated their positions and directions every PRT. The missile evaluated the echo powers from the platform and decoy. After radar processing and filtering, the missile estimated the position and velocity of a target and updated its direction. Given that a target was hit or all targets were missed, the miss distance was calculated, and the simulation was ended. Here, it was determined that the target was hit if its missed distance from the missile was within the proximity fuze range of the missile [14], [15].

The initial condition was set as follows: the missile was oriented towards the intercept point, and its antenna beam was steered to the platform from where the decoy was ejected at $t = 0$ (see Fig. 5). The estimate of the intercept point was important to determine the missile's initial

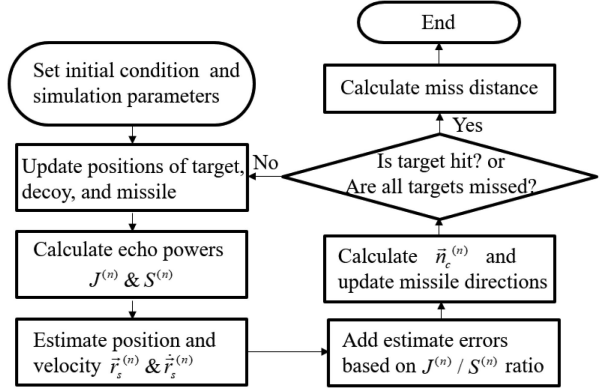


Fig. 4. Flow chart for dynamic simulation.

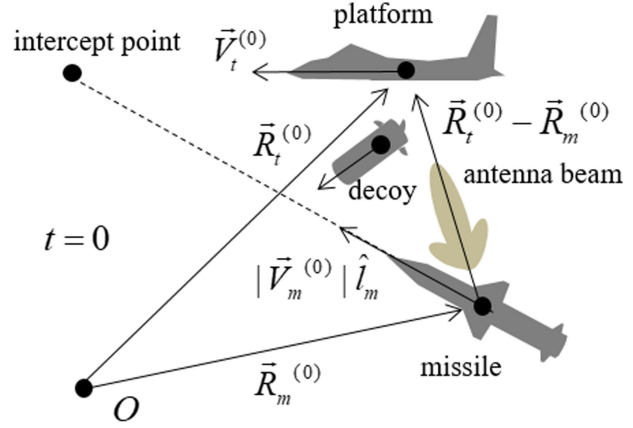


Fig. 5. Initial condition for dynamic simulation.

orientation vector \hat{l}_m . It was assumed that the initial position $\vec{R}_t^{(0)}$ and velocity vector $\vec{V}_t^{(0)}$ of the platform were accurately estimated in order to evaluate the intercept point. The intercept time t_{int} is expressed as

$$t_{int} = \frac{AC \cos \varphi + \sqrt{(AC \cos \varphi)^2 + (B^2 - A^2)C^2}}{B^2 - A^2} \quad (14)$$

where $A = |\vec{V}_t^{(0)}|$, $B = |\vec{V}_m^{(0)}|$, $C = |\vec{R}_t^{(0)} - \vec{R}_m^{(0)}|$, and $\cos \varphi = (\vec{V}_t^{(0)} / |\vec{V}_t^{(0)}|) \cdot (\vec{R}_m^{(0)} - \vec{R}_t^{(0)})$. Note that $B > A$ because the velocity of the missile was generally considerably greater than that of the platform was. Hence, \hat{l}_m was expressed as

$$\hat{l}_m = \frac{\vec{V}_t^{(0)} t_{int} + \vec{R}_t^{(0)} - \vec{R}_m^{(0)}}{|\vec{V}_m^{(0)}| t_{int}}. \quad (15)$$

III. SIMULATION RESULTS

Based on the computational procedure in Fig. 4 and the initial condition in Fig. 5, the miss distance of the platform was computed because it was an important parameter that determined the survivability of the platform. The simulation parameters are summarized in Table I.

TABLE I
Simulation Parameters and Initial Condition

Objects	Parameters	Value or state
Platform	Initial position $\vec{R}_p^{(0)}$	(0,5000,2000) [m]
	Initial velocity $ \vec{V}_p^{(0)} $	Mach 0.8
	Initial orientation $\vec{\gamma}_p^{(0)}$	(0,-1,0)
	Movement	Level flight or sustain turn (2g)
Decoy	Maximum antenna gain G_{ant}	10 dBi
	Power amp gain G_{amp}	15 dB
	HPBW (end-fire)	90°
	Polarization	Circular-pol (CP) or linear-pol (LP)
	Ejection angle in platform's local coordinates (Fig. 6)	$(\theta_0, \phi_0) = (0^\circ, 0^\circ)$
Missile	PRT	1 ms
	Transmit power	10 kW
	Pulse width	1 μ s
	Chirp rate	20 MHz/ μ s
	Initial velocity $ \vec{V}_m^{(0)} $	Mach 3
	Maximum load factor $\max \vec{n}_c $	12g
	Guidance law	Proportional navigation (PN)
	Proximity fuze range R_{fuze}	20 m
	Antenna elements	232
	Antenna spacing	$\lambda/2$ (half-wavelength)
	Maximum antenna gain	30 dBi
	Antenna HPBW	8°
	Polarization	Linear pol

The end-fire beam pattern was considered for the decoy, which was approximated by the Gaussian beam as

$$G(\theta_d) = G_{ant} \exp \left(-4 \ln 2 \times \left(\frac{\cos^{-1}(|\cos \theta_d|)}{\theta_{HPBW}} \right)^2 \right) \quad (16)$$

where θ_d is the angle in the local coordinates of the decoy; θ_{HPBW} and G_{ant} are the HPBW and maximum gain of the antenna, respectively.

To solve the problem involving various missile approach scenarios through simulations, a missile approach angle was defined in the platform's local coordinates at $t = 0$, as shown in Fig. 6.

To analyze the missile trajectory and resulting miss distance, we examined the jamming-to-signal ratio (J/S) and tracking history (see Fig. 7) under following conditions: $R_0 = 5$ km, $\theta_0 = 30^\circ$, and $\phi_0 = 0^\circ$. The platform maneuver was a sustain turn movement, and the decoy's antenna pattern was end fire with a circular polarization (CP). Moreover, $G_{ant} = 10$ dB and $G_{amp} = 15$ dB were assumed.

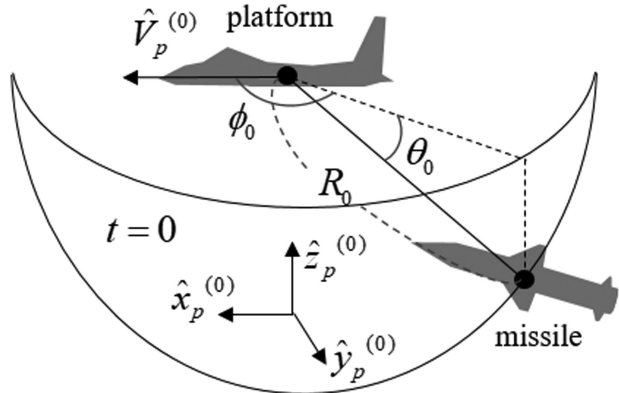


Fig. 6. Initial displacement of missile in platform's local coordinate.

When $t < 1.5$ s, the missile forms a single track where the decoy and platform are unresolved. However, after $t = 1.5$ s, the missile's antenna beam was locked only on the decoy [see Fig. 7(c)]. Thus, the antenna gain towards the decoy, G_{md} , became larger as the main beam was focused on the decoy, which resulted in a large jamming power J [see Fig. 7(b)]. As the missile approached the proximity of the decoy, R_{md} decreased; J dramatically increased because it is proportional to $1/R_{md}^4$. Also, the platform leaves the HPBW of the missile when $t > 3.15$ s. In Fig. 7(b), the fluctuation of J/S during 3 s is due to the variation of the RCS of the platform. The miss distances of the decoy and platform were 255 and 1.2 m, respectively. The platform survived, and the decoy was hit when $t = 4.196$ s. However, it was considerably difficult to consider all possible scenarios. Hence, in the following sections, the simulation of four important cases is considered.

A. Platform Reaction Range

Studies pertaining to the decoy's launch time and launch angles for the successful evasion of incoming missiles [6], [16] have been conducted. It has been observed that the decoy's launch time played an important function in its effectiveness to draw the missile away and thereby enhanced the platform's survivability [16]. In this section, the analysis on how the separation time of the decoy affected survivability is considered. Moreover, the platform's minimum reaction range in order to survive against the missile on an engagement scenario was evaluated.

Considering the fuze range of the missile, the distance between the platform and missile was important when the decoy was deployed. For this simulation, the platform performed the sustain turn maneuver with a Mach 0.8 velocity and 2g acceleration. The missile approached with a Mach 3 velocity from $\theta_0 = 30^\circ$ and $\phi_0 = 0^\circ$ to 90° with $\phi_0 = 10^\circ$ sampling interval (see Fig. 6). The antenna pattern of the decoy, assumed as an end fire with a circular polarization, and other parameters are summarized in Table I. In the scenario, we analyzed the miss distance of the platform for two cases: $R_0 = 1$ km and $R_0 = 3$ km (see Fig. 8). When the platform counteracted the RF missile, which approached from a range of $R_0 = 3$ km, the jamming was efficient for

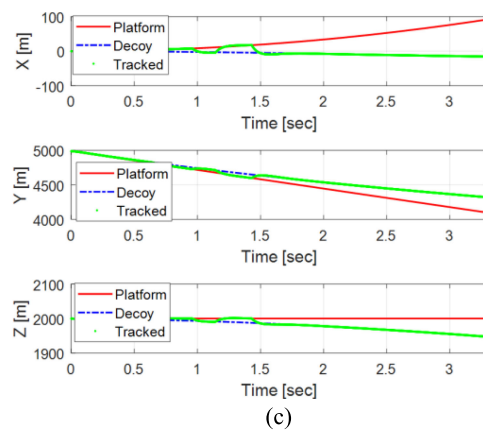
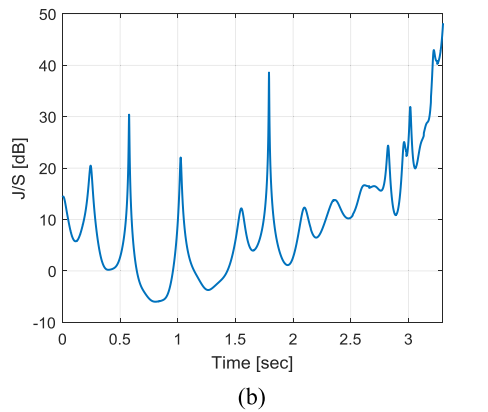
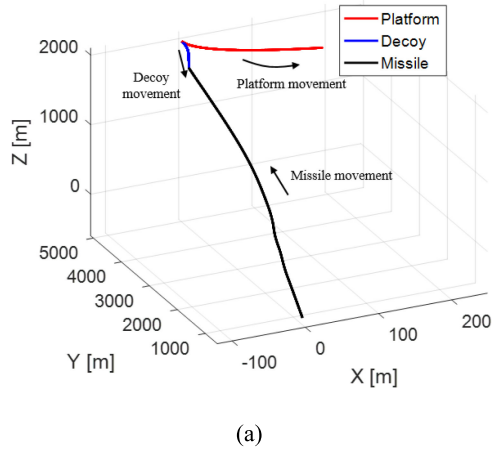


Fig. 7. Missile, platform, and decoy trajectories; jamming-to-signal ratio (J/S). Tracking history when $R_0 = 5 \text{ km}$, $\theta_0 = 30^\circ$, and $\phi_0 = 0^\circ$.

The platform maneuver was a sustain turn movement (2g) and decoy antenna pattern was end fire with circular polarization; $G_{\text{ant}} = 10 \text{ dB}$ and $G_{\text{amp}} = 15 \text{ dB}$. (a) Trajectory. (b) J/S . (c) Tracking history.

approach angles of $\theta_0 = 30^\circ$ and $\phi_0 = 0^\circ$ to 60° . This was reasonable because the jamming power transmitted from the end-fire pattern of the 90° HPBW was mainly focused on the LOS direction. For the case of $R_0 = 3 \text{ km}$, the platform had approximately 2.4 s to react to a Mach 3 missile velocity. For 2.4 s, the separation between the platform and decoy was sufficiently larger than the proximity fuze range R_{fuz} = 20 m (see Fig. 9). Thus, the platform can survive because it was located outside the fuze range R_{fuz} .

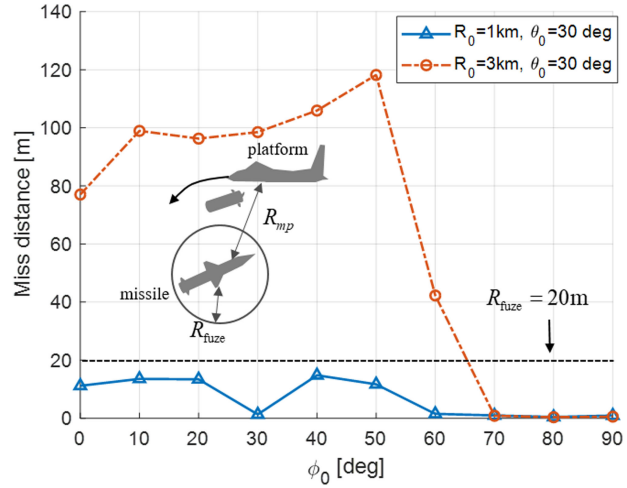


Fig. 8. Miss distance of platform when platform counteracts missile approaching from ranges of 1-km and 3-km.

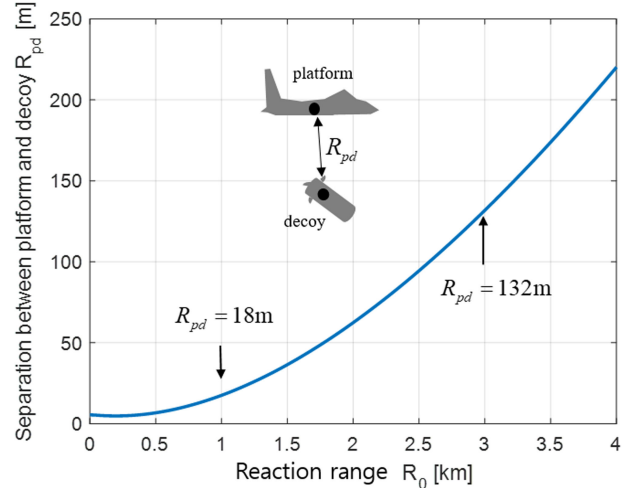


Fig. 9. Separation distance between platform and decoy when platform follows a sustain turn maneuver with 2g acceleration.

However, when the reaction range was reduced to $R_0 = 1 \text{ km}$, the time taken for the missile to approach to the platform was approximately 0.8 s, which was not sufficient for the platform to survive because the platform was within the fuze range, although the missile was redirected to the decoy. The time required for the decoy to be separated from the platform can be calculated based on the missile's velocity and approach range. Given that the separation time was computed, the separation distance between the platform and decoy, R_{pd} , can also be evaluated, as shown in Fig. 9. It was observed that the platform's reaction range R_0 should be 1.2 km, at a minimum, where the separation between the platform and decoy became 25 m. The simulation of the process is clearly illustrated in Fig. 8.

B. Platform Maneuvering

The platform's evasion tactic was one of the effective primary factors to counteract missile attacks [13]. For instance, a typical tactic was to move perpendicular to LOS of the approaching missile [13]. Hence, the sustain turn

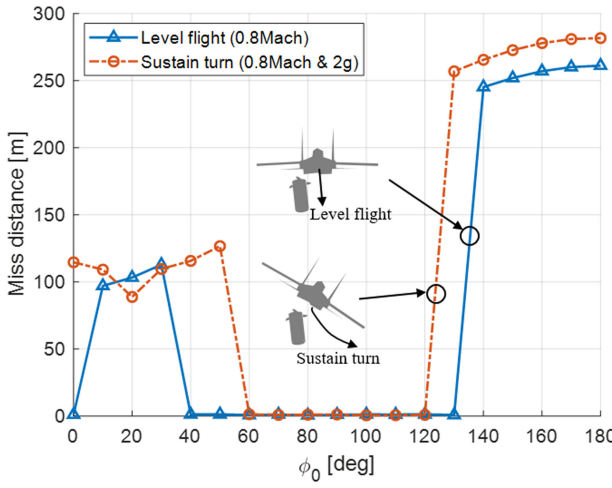


Fig. 10. Miss distance comparison when platform maneuvering is sustain turn (Mach 0.8 with 2g) or level flight (Mach 0.8).

movement with proper acceleration rate may be one of the optimal maneuvers in which the survivability of the platform is maximized because the platform moves normal to the LOS of the missile when it follows the sustain turn maneuvering. In this section, two examples of maneuvers were considered—level flight and sustain turn movement with 2g acceleration. Through simulation, it was shown how and why the platform’s tactical movement affected its survivability. The following scenario was considered for analysis. The missile approached with a Mach 3 velocity from $R_0 = 3$ km, $\theta_0 = 35^\circ$, and $\phi_0 = 0^\circ$ to 180° with a sampling interval of $\phi_0 = 10^\circ$ (see Fig. 6). The decoy’s antenna pattern was assumed as end fire with a circular polarization. Other parameters are summarized in Table I. The miss distance was analyzed for, first, a sustain turn with a Mach 0.8 velocity and 2g acceleration, and second, a level flight with a Mach 0.8 velocity. Different maneuvers generated different radar echo signals from the platform as incidence angles on the platform varied. Fig. 10 shows the miss distance comparison for the two platform maneuvering cases.

For the sustain turn maneuver, the platform survivability was found better than that of the level flight maneuver was. For example, when the missile approached from $R_0 = 3$ km, $\theta_0 = 35^\circ$, and $\phi_0 = 0^\circ$, the miss distances of the platform were 114 and 1.3 m for the sustain turn and level flight maneuvers, respectively. For the sustain turn case, J/S was always larger than 1, and the missile consistently tracked the decoy [see Fig. 11(a)]. The platform’s RCS fluctuated as the angles of incident electromagnetic waves varied when the platform turned. It can be seen that roughly 10 dBsm RCS fluctuation for the sustain turn case as shown in Fig. 11(b) this was because the RCS was very sensitive to the local incident angle in the platform’s local coordinates (see Fig. 3 in [7]). On the other hand, the RCS fluctuation was small for the level flight case because there was little variation of the local incident angle. For the sustain turn case, an RCS reduction of approximately 5 dB was achieved compared to that of the level flight case.

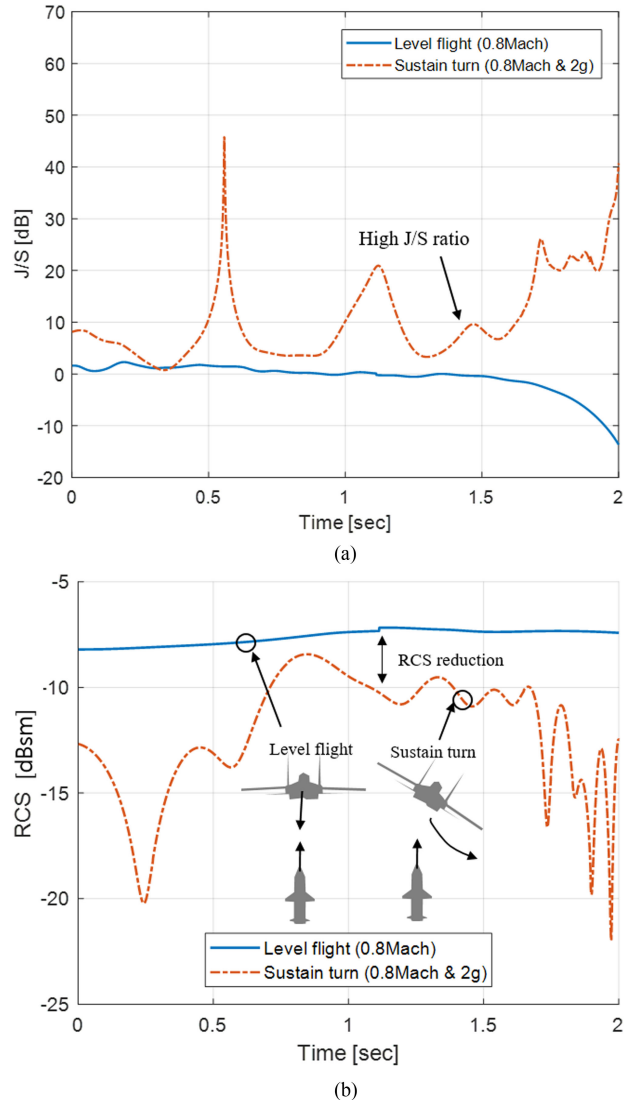


Fig. 11. J/S and RCS variations for 2 s when the missile approached from $R_0 = 3$ km, $\theta_0 = 35^\circ$, and $\phi_0 = 0^\circ$ for level flight and sustain turn maneuvers.

Hence, for the level flight case, large scattered power of the platform was steadily delivered, and the platform’s location was tracked by the missile. Note that the difference when $\phi_0 = 0^\circ$ and $\phi_0 = 10^\circ$ for the level flight case in Fig. 10 was because the RCS observed by the missile when $\phi_0 = 10^\circ$ was approximately 9 dBsm lower than that when $\phi_0 = 0^\circ$, which results in higher J/S and it was able for the platform to survive.

C. Decoy Dynamics

Because decoy dynamics, such as trajectories and moving directions, are extremely important for an efficient ECM, substantial efforts were expended to determine the optimal displacement of the decoy in engagement scenarios [5], [17]. In this section, the effects of decoy dynamics on the jamming performance, especially for a free fall type of decoy, are discussed. For this, the following scenario was considered. Simulation parameters are summarized in

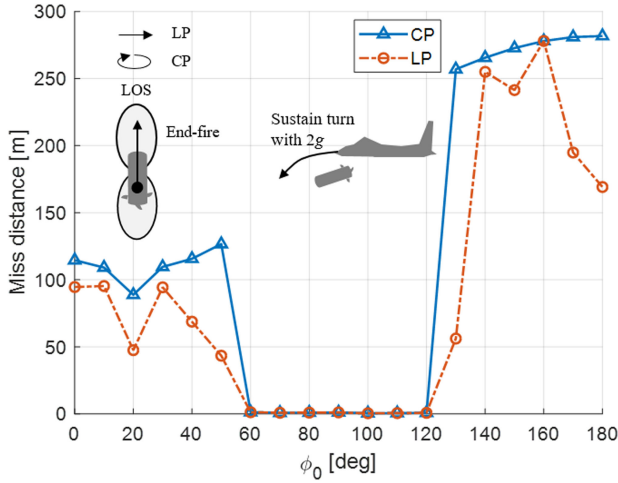


Fig. 12. Miss distance comparison when decoy use LP and CP.

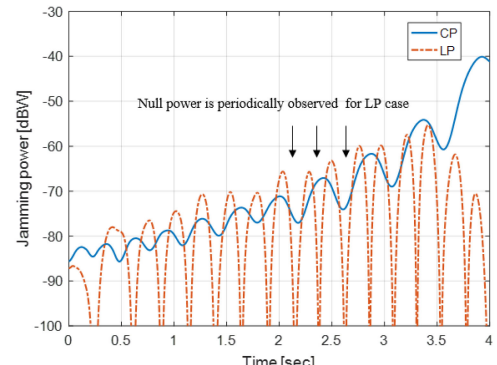
Table I. The missile's approach condition was $R_0 = 3$ km, $\theta_0 = 35^\circ$, and $\phi_0 = 0^\circ$ to 180° . The platform maneuver was assumed as a sustain turn with a $2g$ acceleration. The decoy RF specification was $G_{\text{ant}} = 10$ dB and $G_{\text{amp}} = 20$ dB, end-fire type. For this simulation, two different polarizations were considered for the decoy's antenna: linear polarization (LP) and CP (see Fig. 12).

It was observed that the deception performance of CP was superior to that of LP. The difference was because of the polarization mismatch [9] to which the jamming power was linearly proportional. For example, when $\phi_0 = 30^\circ$ in Fig. 12, the jamming power history and polarization mismatch factor are plotted in Fig. 13.

The jamming power had several null points with LP, whereas that with CP was stable. The platform was directly exposed to the missile at these null points. For the one-link channel, the polarization mismatch factor of CP was 3 dB lower than that of LP. As the decoy was of the repeater type, the channel of interest was the dual link, and CP provided a 6-dB lower jamming performance. However, the jamming power of CP was stable as the decoy continued to fall until it finally achieve an appreciable miss distance. The null points of the polarization mismatch factor was caused by the decoy's rotation. After the decoy was ejected from the platform and fell, its angular trajectory was not static but rotated on its LOS axis (see Fig. 14), which was caused by the circular fins of the decoy. The time taken for a 360° rotation was 0.52 s, and the polarization mismatch occurred every 0.26 s as the mismatch occurred every 180° rotation. Therefore, it was observed that the dynamics of the decoy were key factors that determined the jamming performance of the decoy.

D. Missile's Maximum Load Factor

The maximum load factor of the missile, $|\vec{n}_c|$, which affected the guidance boundary, was generally limited. In this section, because the performance of the ECM technique may considerably depend on the performance of the guidance system, the problem on how the decoy can be operated



(a)

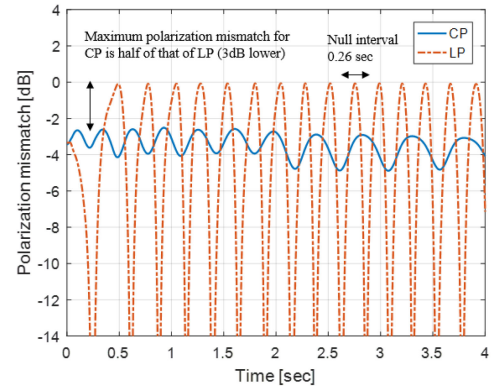


Fig. 13. Comparison of jamming power (J) history and polarization mismatch for CP and LP when $\phi_0 = 30^\circ$. (a) Jamming power history. (b) Polarization mismatch factor.

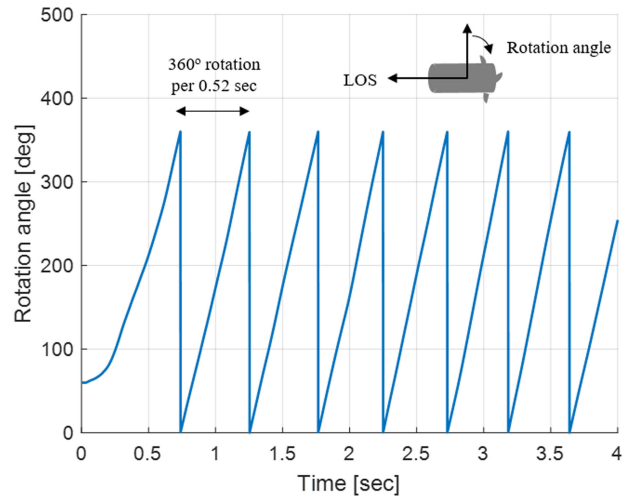


Fig. 14. Rotation angle of decoy with respect to time on its LOS axis.

efficiently using the limitation of the missile's load factor is discussed. Under a Mach 3 velocity, the missile's maneuver range perpendicular to its LOS direction is shown in Fig. 15. As the range along the LOS direction or $|\vec{n}_c|$ decreased, the maneuver range also decreased.

The scenario shown in Fig. 10, where the platform maneuvering was the sustain turn with a Mach 0.8 velocity

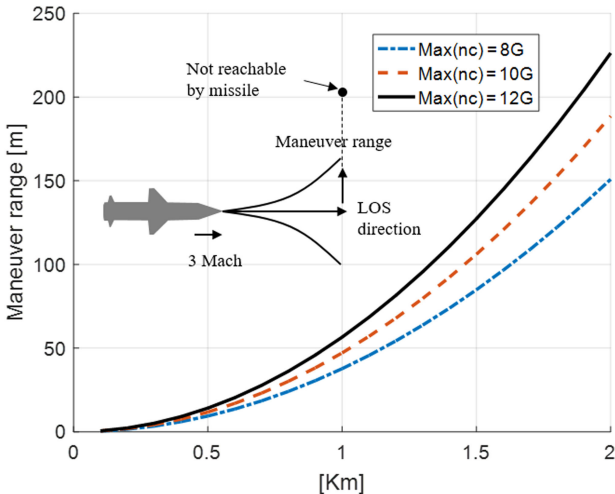
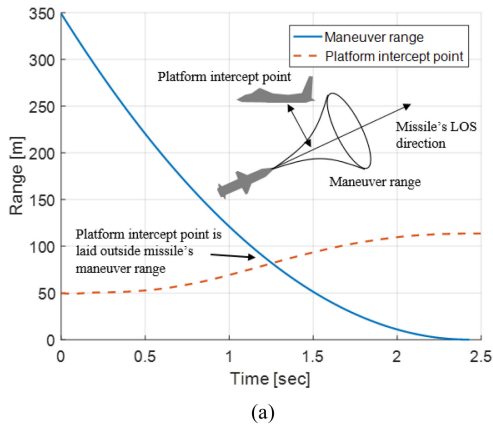
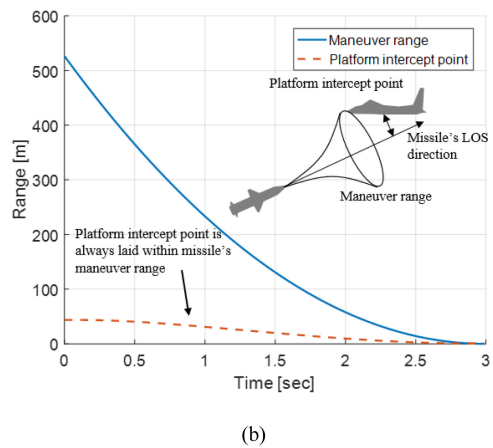


Fig. 15. Maneuver range of missile with different maximum load factor.



(a)

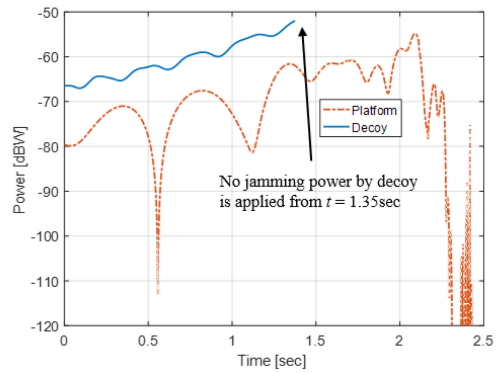


(b)

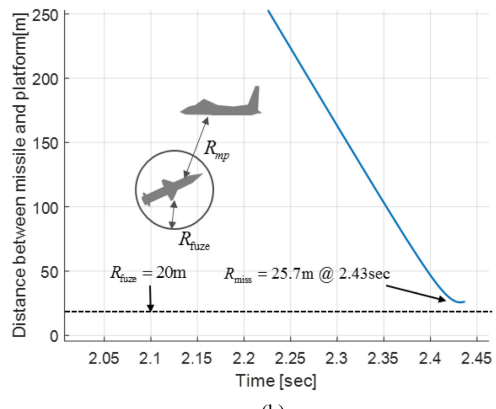
Fig. 16. Analysis of perpendicular ranges from missile's LOS axis to platform intercept point for platform survival and death cases.

(a) Survival case. (b) Death case.

and 2g acceleration, was also considered. The missile approached from $R_0 = 3 \text{ km}$ and $\theta_0 = 35^\circ$ with a Mach 3 velocity. As shown in the Fig. 10, the platform can survive when $\phi_0 = 0^\circ$ but not when $\phi_0 = 90^\circ$. Fig. 16 shows the analyses of perpendicular ranges from the missile's LOS axis to the platform intercept point for the survival and death cases. For the platform survival case ($\phi_0 = 0^\circ$), it



(a)



(b)

Fig. 17. Jamming power off and miss distance analysis. (a) Power history. (b) Distance between missile and platform.

was observed that the intercept point of the platform was outside of the missile's maneuver and fuze ranges at certain times. The time when the platform was outside of the maneuver range and margin of the fuze range was 1.35 s. This meant that the survivability of the platform was guaranteed starting from 1.35 s, even without jamming, because the missile was no longer able to reach the intercept point. On the other hand, for the platform death case ($\phi_0 = 90^\circ$), the platform intercept point remained within the missile's maneuver range.

The optimal power consumption was determined based on these analyses. Taking into consideration the fact that the jamming power of the decoy was not supplied starting from the 1.35 s time shown in Fig. 16(a), the miss distance was 25.7 m in 2.43 s, which was larger than the fuze range of the missile (see Fig. 17). Thus, for this case, the platform can survive when the jamming power lasted for 1.35 s. Accordingly, it was advantageous that the large jamming power (larger than platform's scattered power) applied by the decoy lasted until the platform's intercept point was outside the missile's maneuvering boundary.

E. Evaluation of Platform Survival Probability

The estimated errors in the RF missile depended on the signal-to-noise ratio (SNR). These errors were expressed

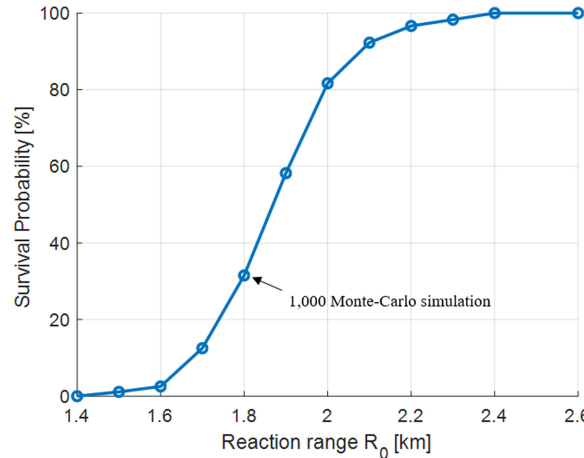


Fig. 18. Survival probability of platform with respect to the platform's reaction range from 1.4 to 2.6 km with a 200-m sampling interval.

as [18]

$$\sigma_{\text{range}} \approx \frac{c}{2\text{BW}\sqrt{2\text{SNR}}}, \quad \sigma_{\text{angle}} \approx \frac{\theta_{\text{HPBW}}}{k_m\sqrt{2\text{SNR}}} \quad (17)$$

where σ_{range} and σ_{angle} are the range and angular errors, respectively; BW and c are the system bandwidth and speed of light, respectively; k_m is the normalized monopulse slope, which was set to 1.56. Because we were interested in the ratio of return powers between the platform (S) and decoy (J), SNR is identical to the J/S ratio. For every PRT, SNR was computed, and estimated errors were added during the dynamic simulation (see Fig. 4). Through the Monte Carlo simulation with 1000 realizations, the survival probability of the platform was simulated. If the platform's miss distance was greater than the fuze range of the missile, then, it was considered that the platform survived.

In the identical scenario in Fig. 8, the platform's survival probability was calculated with respect to its reaction range (1.4–2.6 km), with a 200-m sampling interval. Considering the estimation errors in the missile's processing, the platform's reaction range was 2.0 km to achieve an 80% survival probability (see Fig. 18). According to the result in Fig. 9, when the platform's reaction range was 2.0 km, the separation between the platform and decoy was 63 m.

The scenario that the missile approached from $R_0 = 5$ km, $\theta_0 = 30^\circ$, and $\phi_0 = 0^\circ$ was considered. The sustain turn and level flight maneuvers of the platform were compared when the decoy's antenna gain and HPBW were 10 dB and 90° , respectively. The decoy's polarization was assumed as CP. The survival probability was simulated with respect to the decoy's amplifier gain, which varied from 0 to 16 dB with a 2-dB sampling interval, as shown in Fig. 19.

With the sustain turn maneuver, the platform's survivability was higher than that of the level flight maneuver under the same amplifier gain. For an 80% survival probability, the required amplifier gains were approximately 4 and 8 dB for the sustain turn and level flight maneuvers, respectively. The 4-dB amplifier gain between the two was because of the effect of RCS reduction, which occurred

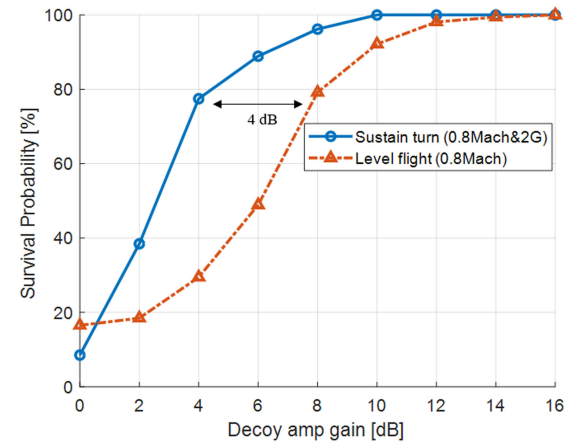


Fig. 19. Survival probability of platform with respect to decoy's amplifier gain from 0 to 16 dB with a 2-dB sampling interval: sustain turn versus level flight.

with the sustain turns of the platform, as mentioned earlier in Section III-B.

IV. CONCLUSION

Several important problems regarding the airborne platform, repeater-type decoy, and RF missile that affected the deception of an active RF missile system were analyzed. Through a numerical simulation, several important problems pertaining to the platform reaction range, platform maneuvering, decoy dynamics, and missile maximum load factor were solved. The analyses of these problems are summarized as follows.

When the platform ejected the decoy, the separation between them increased in a quadratic order with respect to time. Their separation should be greater than the proximity fuze range of the missile when the missile reached the vicinity of the decoy. Otherwise, because the platform was within the fuze range, the platform's survivability cannot be guaranteed even though the decoy effectively deceived the missile. In our simulation it was observed that the platform should react when the missile is at least 1.2 km away, at which instance, the separation of the platform and decoy was 25 m when the platform followed a 2g sustain turning with a Mach 0.8 velocity and initially ejected the decoy towards the forward direction. We observed that the platform maneuvering caused an RCS variation, which affected the return power received by the missile. For the sustain turn maneuvering case, an approximately 5-dB RCS reduction was observed in the scenario, compared to that of the level flight case. By deploying the end-fire decoy with a sustain turn maneuver, the platform's survivability was observed for a wider range of missile approach angles. It was determined that the dynamics of the decoy had a significant impact on RF characteristics, on which jamming performance depended. For instance, when the decoy was ejected from the platform, the decoy rotated along its LOS direction. The rotation caused a degradation of the jamming performance when the decoy adopted LP because the occurrence of the polarization mismatch depended on half of

the rotation period, which caused the jamming power to periodically become null. With CP, the polarization mismatch can be prevented though the jamming power for CP was totally reduced by 6 dB. It was noted that it was effective for the decoy to employ CP for the end-fire beam type as the stable jamming power is exerted. Regarding the guidance law of the missile, the maximum load factor limited its maneuvering boundary. By comparing the platform survival and death cases, it was observed that the platform's intercept point was always within the missile's maneuvering boundary for the death case, whereas the platform's intercept point was outside the boundary at some time for the survival case. Based on this, the decoy's efficient operation was determined. For instance, it was monitored that the missile cannot be guided toward the platform when the platform leaves the maneuver boundary of the missile. Upon this fact, it may be possible to optimize the jamming duration to make best use of energy available given that the time when the platform will exit the missile's maneuver boundary.

Furthermore, the survival probability of the platform was evaluated through the Monte Carlo simulation, in which estimated errors in the missile's radar system were considered. In an engagement scenario, in which the missile approached from the forward direction, and the platform turned with a 2g acceleration and Mach 0.8 velocity, it was concluded that the platform's reaction range should be 2.0 km, at a minimum, to achieve a survival probability above 80%. It was also observed that the sustain turn maneuver required a 4-dB lower decoy amplifier gain than the level flight maneuver did for 80% of the survival probability. As anticipated, a 4-dB power enhancement followed the details in the platform maneuvering problem.

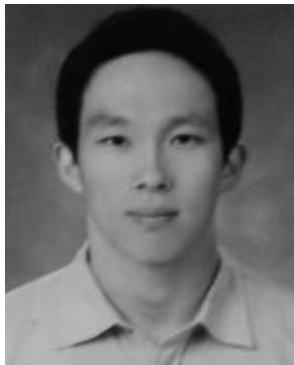
Based on the analyses addressed in this paper, the optimal parameters of the EAD and tactical management of the platform can be drawn to maximize the survivability of the platform.

ACKNOWLEDGMENT

The authors would like to thank Aerodynamic Analysis & Design Laboratory members, including Dr. C. Baek and Prof. S. Lee at Inha University, as they have offered access to the dynamic database of the active decoy and airborne platform.

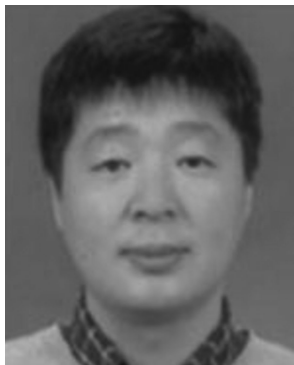
REFERENCES

- [1] F. Neri
Introduction to Electronic Defense Systems, 3rd ed. Rijeka, Croatia: SciTech, 2018.
- [2] F. Neri
Anti-monopulse jamming techniques
In *Proc. SBMO/IEEE Int. Microw. Optoelectronics Conf.*, 2001, vol. 2, pp. 45–50.
- [3] Z. Song, H. Xiao, Y. Zhu, and Z. Lu
A novel approach to detect the unresolved towed decoy in terminal guidance
Chin. J. Electron., vol. 21, no. 2, pp. 367–373, 2012.
- [4] W. J. Kerins
Analysis of towed decoys
IEEE Trans. Aerosp. Electron. Syst., vol. 29, no. 4, pp. 1222–1227, Oct. 1993.
- [5] W. Zhou, J. Luo, Y. Jia, and H. Wang
Performance evaluation of radar and decoy system counteracting antiradiation missile
IEEE Trans. Aerosp. Electron. Syst., vol. 47, no. 3, pp. 2026–2036, Jul. 2011.
- [6] E. V. Lakshmi, N. N. Sastry, and B. P. Rao
Optimum active decoy deployment for effective deception of missile radars
In *Proc. IEEE CIE Int. Conf. Radar*, , 2011, vol. 1, pp. 234–237.
- [7] J. W. Rim, K. H. Jung, I. S. Koh, C. Baek, S. Lee, and S. H. Choi
Simulation of dynamic EADs jamming performance against tracking radar in presence of airborne platform
Int. J. Aeronautical Space Sci., vol. 16, no. 3, pp. 475–483, 2015.
- [8] L. Sun and W. Huo
6-DOF integrated adaptive backstepping control for spacecraft proximity operations
IEEE Trans. Aerosp. Electron. Syst., vol. 51, no. 3, pp. 2433–2443, 2015.
- [9] D. M. Pozar
Microwave Engineering. Hoboken, NJ, USA: Wiley, 2012.
- [10] Y. Zheng, S. M. Tseng, and K. B. Yu
Closed-form four-channel monopulse two-target resolution
IEEE Trans. Aerosp. Electron. Syst., vol. 39, no. 3, pp. 1083–1089, Jul. 2003.
- [11] B. R. Mahafza
Radar Signal Analysis and Processing Using MATLAB, London, U.K.: Chapman & Hall, 2016.
- [12] D. Tenne and S. Tarunraj
Characterizing performance of α - β - γ filters
IEEE Trans. Aerosp. Electron. Syst., vol. 38, no. 3 pp. 1072–1087, Jul. 2002.
- [13] P. Zarchan
Tactical and Strategic Missile Guidance, Washington, DC, USA: Amer. Inst. Aeronaut. Astronaut., 2012.
- [14] L. Brown
The proximity fuze
IEEE Aerosp. Electron. Syst. Mag., vol. 8, no. 7, pp. 3–10, Jul. 1993.
- [15] J. H. Choi, M. S. Jung, and K. W. Yeom
A design and assessment of a direction finding proximity fuze sensor
IEEE Sensors J., vol. 13, no. 8, pp. 3079–3089, Aug. 2013.
- [16] R. Ragesh, A. Ratnoo, and D. Ghose
Analysis of evader survivability enhancement by decoy deployment
In *Proc. Amer. Control Conf.*, 2014, pp. 4735–4740.
- [17] Y. Chen, H. Wang, and Y. Zhao
Optimal trajectory for swim-out acoustic decoy to countermeasure torpedo
In *Proc. 4th Int. Workshop Adv. Comput. Intell.*, Wuhan, China, pp. 86–91, 2011.
- [18] S. M. Sherman and D. K. Barton
Monopulse Principles and Techniques, Norwood, MA, USA: Artech House, 2013.



Jae-Won Rim received the B.S. and M.S degrees in electronic engineering from Inha University, Incheon, South Korea, in 2014 and 2016, respectively. He is currently working toward the Ph.D. degree at the Department of Electronic Engineering, Inha University, Incheon, South Korea.

His research interests include modeling and simulation for radar system, electronic warfare, and numerical methods in electromagnetic fields.



Il-Suek Koh received the B.S. and M.S. degrees in electronic engineering from Yonsei University, Seoul, South Korea, in 1992 and 1994, respectively, and the Ph.D. degree in Electrical Engineering from the University of Michigan, Ann Arbor, MI, USA, in 2002.

In 1994, he joined LG Electronics Ltd., Seoul, as a Research Engineer. He is currently a Professor with Inha University, Incheon, South Korea. His research interests include wireless communication channel modeling and numerical and analytical methods for electromagnetic fields.